British Journal of Pharmacology

British Journal of Pharmacology (2018) **175** 1590–1606 1590

RESEARCH PAPER

1,3,6,7-Tetrahydroxy-8-prenylxanthone ameliorates inflammatory responses resulting from the paracrine interaction of adipocytes and macrophages

Correspondence Ligen Lin, State Key Laboratory of Quality Research in Chinese Medicine, Institute of Chinese Medical Sciences, University of Macau, Avenida da Universidade, Taipa, Macau, China. E-mail: ligenl@umac.mo

Received 7 September 2017; **Revised** 29 December 2017; **Accepted** 18 January 2018

Dan Li[1], Qianyu Liu[1], Wen Sun[1], Xiuping Chen[1], Ying Wang[1], Yuxiang Sun[2] and Ligen Lin[1]

[1]*State Key Laboratory of Quality Research in Chinese Medicine, Institute of Chinese Medical Sciences, University of Macau, Taipa, Macau, China, and* [2]*Department of Nutrition and Food Science, Texas A&M University, College Station, TX, USA*

BACKGROUND AND PURPOSE

Chronic inflammation in adipose tissue is critical in the onset and development of insulin resistance and type 2 diabetes. Macrophage infiltration into adipose tissue and pro-inflammatory polarization play key roles in adipose tissue inflammation. The fruit hull of mangosteen (*Garcinia mangostana*) is used in traditional medicine to treat various inflammatory diseases. However, its role in regulating adipose tissue inflammation is unexplored. This study was designed to identify xanthones from *G. mangostana*, which could ameliorate adipose tissue inflammation.

EXPERIMENTAL APPROACH

Expressions of inducible NOS, cytokines, chemokines and components of the NF-κB and MAPKs pathways were evaluated using Western blotting, immunofluorescence, quantitative real-time PCR or ELISA. The migration of macrophages towards adipocytes was tested using Transwell experiments *in vitro*. A murine model of LPS-induced acute inflammation was used to examine effects of 1,3,6,7-tetrahydroxy-8-prenylxanthone (TPX) on inflammatory responses in adipose tissue *in vivo*.

KEY RESULTS

From a series of xanthones isolated from *G. mangostana*, TPX was identified as a potent inhibitor of LPS-induced NO production and IL-6 secretion in RAW264.7 macrophages. TPX ameliorated LPS-induced inflammatory responses in RAW264.7 macrophages, and TNF-α-mediated inflammation in 3T3-L1 adipocytes, through inhibiting MAPKs and NF-κB activation and promoting sirtuin 3 expression. TPX also blocked RAW264.7 macrophages migration towards 3T3-L1 adipocytes in co-cultures. Furthermore, TPX alleviated LPS-induced adipose tissue inflammation *in vivo* by reducing pro-inflammatory cytokines and preventing the pro-inflammatory polarization of macrophages.

CONCLUSIONS AND IMPLICATIONS

Taken together, our results indicate that TPX disrupts the inflammatory responses between macrophages and adipocytes, and attenuates adipose tissue inflammation.

Abbreviations

Ccl11, chemokine (C-C motif) ligand 11; CM, conditioned media; Cxcl10, C-X-C motif chemokine 10; DAPI, 4′, 6-diamidino-2-phenylindole; iNOS, inducible NOS; MCP-1, monocyte chemotactic protein-1; MIP-1α, macrophage inflammatory protein 1-α; SIRT3, sirtuin3; TPX, 1,3,6,7-tetrahydroxy-8-prenylxanthone.

DOI:10.1111/bph.14162

Introduction

Chronic low-grade inflammation in adipose tissue, characterized as elevated circulating cytokines levels, such as TNF-α, IL-6 and monocyte chemotactic protein-1 (**MCP-1**; also known as CCL2) and adipose tissue derangements, plays a key role in the onset and development of **insulin** resistance and type 2 diabetes (Weisberg *et al.,* 2003; Shoelson *et al.,* 2006; Hosogai *et al.,* 2007). Macrophages that infiltrate the adipose tissue, not adipocytes, produce the majority of cytokines in response to obesity (Weisberg *et al.,* 2003). These macrophages consist of classically activated macrophages (M1) and alternatively activated macrophages (M2). M1 macrophages, expressing both F4/80 and CD11c but not CD206, produce pro-inflammatory cytokines. M2 macrophages, expressing F4/80 and CD206 but not CD11c, produce anti-inflammatory cytokines, such as **arginase 1** (ARG1; Lumeng *et al.,* 2007; Zeyda and Stulnig, 2007). There is emerging evidences indicating that the infiltration of macrophages and M1 macrophages polarization in adipose tissue are the major pathogenic factors involved in insulin resistance (Weisberg *et al.,* 2003; Hosogai *et al.,* 2007; Lumeng *et al.,* 2007). Adipose tissue inflammation is the major pathogenic factor for the development of insulin resistance compared to hepatic inflammation in diet-induced obese mice (van der Heijden *et al.,* 2015). Therefore, ameliorating adipose tissue inflammation may provide a promising therapeutic strategy for treatment of insulin resistance and type 2 diabetes.

Adipose tissue inflammation is a dynamic processes controlled by multiple mechanisms. Chemokines are a superfamily of small proteins with an important role in inflammatory reactions (Mantovani *et al.,* 2004). Chemokines are involved in cellular interactions and tropism in situations frequently associated with inflammation (Lazennec and Richmond, 2010). Chemokines secreted from adipose tissue, such as MCP-1 and macrophage inflammatory protein 1-α (**MIP-1α**; also known as CCL3), recruit circulating monocytes into adipose tissues, where they then differentiate into macrophages. MCP-1 also promotes the proliferation of macrophages in adipose tissue *in situ* (Amano *et al.,* 2014). NF-κB, a transcriptional factor of pro-inflammatory cytokines, mediates adipose tissue inflammation (Vitseva *et al.,* 2008). Activation of MAPKs in adipocytes also increases the secretion of pro-inflammatory cytokines (Johnson and Lapadat, 2002). In addition, altering the inflammatory signalling in macrophages, through NF-κB and MAPKs pathways, has been shown to be sufficient to modulate adipose tissue inflammation (Wellen and Hotamisligil, 2005; Bensinger and Tontonoz, 2008). Sirtuins are NAD^+-dependent deacetylases, and there are seven sirtuin isoforms (SIRT1 to 7) in mammalian cells. **SIRT3** is primarily located in mitochondria and plays an anti-inflammatory role in macrophages (Xu *et al.,* 2016).

Mangosteen (*Garcinia mangostana*) is a type of tree that is widely distributed in Southeast Asia. The fruit hull of mangosteen has been used as a traditional anti-inflammatory agent, to treat skin infections, wounds and diarrhoea (Tewtrakul *et al.,* 2009). An extract of mangosteen was reported to have an anti-inflammatory effect on dextran sulfate sodium-induced colitis in mice (Chae *et al.,* 2017). α-Mangostin and γ-mangostin are the major xanthones from *G. mangostana* that have been demonstrated to have an anti-inflammatory effect (Chen *et al.,* 2008; Tewtrakul *et al.,* 2009). In the present study, a series of xanthones from *G. mangostana* were screened and 1,3,6,7-tetrahydroxy-8-prenylxanthone (TPX) was identified to inhibit **LPS**-induced inflammatory responses in RAW264.7 macrophages and TNF-α-induced inflammation in 3T3-L1 adipocytes, and to suppress adipose tissue inflammation in LPS-treated mice.

Methods

Cell culture

Mouse-derived RAW264.7 macrophages (American Type Culture Collection, Manassas, VA, USA) were cultured in DMEM with 10% FBS. Cells were maintained in a humidified incubator with 5% CO_2 at 37°C.

3T3-L1 pre-adipocytes (American Type Culture Collection) were grown in DMEM supplemented with 10% FBS in a humidified incubator with 5% CO_2 at 37°C. 3T3-L1 cells were induced to differentiate as reported previously (Lin *et al.,* 2012). Briefly, 2 day post-confluent 3T3-L1 pre-adipocytes were stimulated for 72 h with 0.5 mM **IBMX**, 1 μM **dexamethasone** and 5 $\mu g \cdot mL^{-1}$ insulin in DMEM supplemented with 10% FBS. Cells were subsequently treated with DMEM supplemented with 10% FBS and 5-$\mu g \cdot mL^{-1}$ insulin. The differentiation of 3T3-L1 cells was confirmed by microscopic observation and Oil-Red O staining as described previously (Christy *et al.,* 1989; Kohn *et al.,* 1996). After being fully differentiated, adipocytes were pre-incubated with TPX for 6 h and then incubated with TNF-α (15 $ng \cdot mL^{-1}$) for the indicated time. All treatments were performed on day 8 of differentiation.

Macrophage migration assay

Migration assays were performed using Transwell inserts with an 8 μm membrane pore size (Millipore). 3T3-L1 adipocytes were pre-incubated with or without TPX (20 μM) for 6 h. Subsequently, the adipocytes were incubated with TNF-α (15 $ng \cdot mL^{-1}$) for 24 h. RAW264.7 macrophages were seeded onto the inserts at a density of 5×10^4 cells per well. The 3T3-L1-conditioned media (CM) were transferred to 24 well plates containing inserts. After migration for 4 h at 37°C, the macrophages in the lower compartment were fixed with 4% formaldehyde for 20 min and counted as described previously (Marcotorchino *et al.,* 2012).

After being fully differentiated, 3T3-L1 adipocytes were further incubated with migration media (serum free, 0.2% endotoxin and free fatty acid-free BSA in DMEM) for 24 h, and then the CM was transferred to 24 well plates containing inserts. The RAW264.7 macrophages were pre-incubated with or without TPX (20 μM) for 4 h. Subsequently, the RAW264.7 macrophages were seeded onto the inserts at a density of 5×10^4 cells per well. After migration for 4 h at 37°C, the macrophages in the lower compartment were fixed and counted as described above.

LPS-induced adipose tissue inflammation mice model

All animal experiments were approved by the Animal Ethical and Welfare Committee of University of Macau (No. ICMS-

AEC-2014-06). All procedures involved in the animal experiments were carried out in accordance with the approved guidelines and regulations. Animal studies are reported in compliance with the ARRIVE guidelines (Kilkenny *et al.,* 2010; McGrath and Lilley, 2015). Male C57BL/6 mice (8–10 weeks old) were obtained from the Faculty of Health Science, University of Macau (Macau, China). C57BL/6 mice have been shown to be suitable for the generation of a murine model of adipose tissue inflammation model, as induced by a single injection of LPS (Karkeni *et al.,* 2015). The mice were housed in plastic cages with five mice per cage and were fed a regular chow diet (Guangdong Medical Lab Animal Centre, Guangzhou, Guangdong, China) and water *ad libitum* under standard conditions (specific-pathogen-free) with air filtration (22 ± 2°C, 12 h light/12 h dark). To assess the impact of TPX on acute inflammation, the mice were randomly divided into three groups according to body weight (n = 7 in each group). The TPX group of mice were i.p. injected with TPX (20 mg·kg $^{-1}$, dissolved in PEG 400: distilled water, 6:4 vv^{-1}), and the LPS and control group mice were i.p. injected with vehicle solution (PEG 400: distilled water, 6:4 vv^{-1}) once a day for 5 days. On the sixth day, the control group mice were injected i.p. with PBS, and the LPS and TPX group mice were injected i.p. with LPS (4 mg·kg^{-1}, serotype O111:B4). Four hours after the LPS injection, the blood was collected from mice under anaesthesia (inhalation of 3% isoflurane gas at 0.5 L·min^{-1}). Then the mice were euthanized by carbon dioxide inhalation, and the epididymal adipose tissues were dissected and stored at −80°C.

MTT assay

RAW264.7 cells were seeded into 96-well plates at a density of 1 × 10^4 cells per well and incubated overnight. Then the cells were treated with different concentrations of TPX (5, 10 and 20 μM) with or without LPS (1 μg·mL^{-1}) for 24 h. Cell viability was determined by the MTT assay, as described previously (Liu *et al.,* 2016).

Measurement of NO production

RAW264.7 cells were seeded into 24-well plates (1 × 10^5 cells per well) and allowed to adhere for 24 h. The cells were then treated with different concentrations of TPX (5, 10 and 20 μM) or vehicle (DMSO) for 1 h, followed by stimulation with 1 μg·mL^{-1} LPS. DMSO was used as vehicle, with the final concentration of DMSO being maintained at 0.1% of all cultures. After 18 h incubation, the supernatant was collected to determine **NO** content using Griess reagent (Liu *et al.,* 2016).

Real-time RT-PCR

Total RNA was isolated from cells and epididymal adipose tissue using TRIzol Reagent (Invitrogen, Carlsbad, CA, USA), following the manufacturer's instructions. The cDNA was synthesized from 1 μg RNA using the SuperScript III First-Strand Synthesis System for RT-PCR. The qPCR experiments were conducted on Step-One plus real-time PCR System using SYBR green PCR Master Mix with gene specific primers (Supporting Information Table S1). The 18S RNA was used as an internal control.

Western blot analysis

Western blot analysis was performed as described previously (Wang *et al.,* 2016). In brief, protein concentration was measured using a BCA protein assay kit. Equal amounts of protein (15–30 μg) were separated by SDS-PAGE and transferred to PVDF membranes (Bio-Rad, Hercules, CA, USA). After being blocked with 5% non-fat milk for 1 h, the blots were probed with specific primary antibodies (Supporting Information-Table S2) overnight at 4°C and then incubated with horseradish peroxidase conjugated secondary antibody for 1 h at room temperature. The immune-blotting signals were detected using SuperSignal West Femto Maximum Sensitivity Substrate under visualization in a ChemiDoc™ MP Imaging System (Bio-Rad). The intensity of individual bands of the Western blots was quantified using Image J densitometry software and expressed relative to a reference protein signal, as a measure of relative abundance of protein in the different samples. The relative abundance of the TPX-treated groups was then normalized to that of the model group (LPS alone, set as 1.0).

Determination of cytokines

The cell medium and mice serum were centrifuged at 1500 *g* for 10 min at 4°C, and the supernatant was collected. The cell medium, mice serum and epididymal adipose tissue lysates were used for the determination of TNF-α, IL-6 and MCP-1 using commercial ELISA kits, according to the manufacturer's instructions. The cytokine levels in epididymal adipose tissue were further normalized to protein content.

Luciferase reporter assay

The pNFκB-Luc pathway reporter, containing NF-κB binding sites in the promoter region, was purchased from Addgene. RAW264.7 cells cultured overnight in 3.5 cm dish were transfected with an NF-κB luciferase reporter gene or a wild-type Renilla luciferase control reporter vector (pRL-TK) at a ratio of 50:1 in serum-free DMEM for 6 h using TurboFect Transfection Reagent (Thermo Scientific), according to the manufacturer's instructions. After 16 h of transfection, the cells were seeded overnight in a 24-well plate at a density of 1 × 10^5 cells per well. Then the cells were pretreated with TPX (20 μM) for 1 h followed by stimulation with LPS (1 μg·mL^{-1}) for 1 h. The cells were lysed for the Firefly/Renilla luciferase activity assay using a dual-luciferase assay kit (Promega, Madison, WI, USA). The luminescence intensities of firefly luciferase and Renilla luciferase were measured with SpectraMax M5 microplate reader (Molecular Devices, Sunnyvale, CA, USA), and the transcriptional activity was determined by the ratio of firefly luciferase to Renilla luciferase.

NF-κB immunofluorescence

After being incubated on chamber slides overnight, RAW264.7 cells were pretreated with TPX (20 μM) for 1 h and then stimulated with LPS (1 μg·mL^{-1}) for 1 h. The cells were fixed immediately in 4% formaldehyde for 20 min, washed with PBS (pH 7.4) and then permeabilized with 0.5% Triton X-100 (Bio-Rad) for 20 min at room temperature. The slides were then incubated with a primary antibody against NF-κB p65 (1:100 dilution) at 4°C overnight. The slides were washed with PBS and incubated with Texas Red-

conjugated anti-rabbit IgG secondary antibody at 1:1000 dilution at room temperature for 1 h. Finally, the slides were washed and stained with 4′,6-diamidino-2-phenylindole (**DAPI**) for the nuclei of cells. The translocation of p65 into the nucleus was determined by confocal microscopy (Olympus, Tokyo, Japan).

Silencing of SIRT3 in macrophages

The shRNA targeting SIRT3 (mouse, sc-61556), scrambled shRNA (mouse, sc-108060) and shRNA transfection reagent (sc-108061) were purchased from Santa Cruz Biotechnology (Santa Cruz, CA, USA). RAW264.7 cells at 50% confluency were transfected with 4 μg shRNA for 6 h according to the manufacturer's protocol. Cells were switched to fresh medium and incubated for an additional 42 h. Then cells were selected with 10 $\mu g \cdot mL^{-1}$ puromycin for 14 days. Thereafter, cells were pooled together for further experiments.

Statistical analysis

The data and statistical analysis comply with the recommendations on experimental design and analysis in pharmacology (Curtis *et al.,* 2015). The operator and data analysis were blinded. Data were analysed using GraphPad Prism 6.0 software. All experimental data are presented as mean ± SEM, and each experiment was performed a minimum of three times. Significant differences between groups were determined using a one-way ANOVA with Dunnet's multiple comparisons test; $P < 0.05$ was considered to represent a significant difference.

Materials

DMEM and puromycin were purchased from Life Technologies/Gibco Laboratories (Grand Island, NY, USA). FBS was obtained from HyClone (Logan, UT, USA). LPS (*Escherichia coli*, serotype 0111: B4), DAPI, IBMX, dexamethasone, insulin and Griess reagent were purchased from Sigma-Aldrich (St. Louis, MO, USA). ELISA kits for MCP-1, IL-6 and TNF-α were obtained from Neobioscience (Shenzhen, China). Antibodies against **iNOS**, **COX-2**, SIRT3, p65, p-p65, p-**IKK-α**/β, IKK-α, **IKK-β**, p-IκB-α, IκB-α, p-**p38**, p38, p-**ERK** and **ERK** were purchased from Cell Signaling Technologies (Beverly, MA, USA). Antibodies against p-**JNK**, JNK, **PPARα**, **PPARβ**, **PPARγ**, α-tubulin, GAPDH and histone H3 were obtained from Santa Cruz Biotechnology (Santa Cruz, CA, USA). Oligonucleotide primers, SuperScript III First-Strand Synthesis System and TRIzol Reagent were purchased from Invitrogen (Carlsbad, CA, USA). BCA protein assay kit, SYBR green PCR Master Mix, TurboFect Transfection Reagent and SuperSignal West Femto Maximum Sensitivity Substrate were obtained from Life Technologies/Thermo Fisher Scientific (Grand Island, NY, USA). Plasmids of pNF-κB-luc and pRL-TK were purchased from Addgene (Cambridge, MA, USA). The dual-luciferase assay kit was obtained from Promega (Madison, WI, USA). Triton X-100, PVDF membranes were purchased from Bio-Rad (Hercules, CA, USA). TPX was separated from the pericarps of *G. mangostana* (Liu *et al.,* 2016), and its purity was determined to be ≥99.8% by HPLC-UV and ^{1}H NMR spectrum (Supporting Information Figure S1).

Nomenclature of targets and ligands

Key protein targets and ligands in this article are hyperlinked to corresponding entries in http://www.guidetopharmacology.org, the common portal for data from the IUPHAR/BPS Guide to PHARMACOLOGY (Harding *et al.,* 2018) and are permanently archived in the Concise Guide to PHARMACOLOGY 2017/2018 (Alexander *et al.,* 2017a,b).

Results

Identification of anti-inflammatory xanthones from the pericarps of G. mangostana

Fourteen xanthones from the pericarps of *G. mangostana* were chosen (Supporting Information Table S3). First, the non-cytotoxic concentrations of these xanthones on RAW264.7 cells were evaluated by the MTT assay, to determine the maximum safe dosage (Supporting Information Table S3). Next, the anti-inflammatory effect of the above xanthones was evaluated by determining their effects on LPS-stimulated NO production and IL-6 secretion in RAW264.7 cells. TPX (Figure 1A) was the only one with an inhibitory effect in both assays (Supporting Information Figure S2A, B). In these assays, indomethacin was used as a positive control and had IC_{50} values of 3.9 ± 0.3 and 5.1 ± 0.1 μM on NO production and IL-6 secretion, respectively. TPX had no observable effect on cell viability up to 20 μM, with or without the presence of LPS (Supporting Information Figure S2C, D). Therefore, TPX was the only compound that was investigated further.

TPX suppresses LPS-stimulated inflammatory responses in RAW 264.7 cells

The anti-inflammatory effect of TPX was investigated in LPS-stimulated RAW264.7 cells. TPX inhibited NO production in a dose-dependent manner (Figure 1B). Real-time RT-PCR analysis revealed TPX treatment significantly suppressed the LPS-induced increase in iNOS mRNA (Figure 1C). Consistently, TPX reversed LPS-induced increase in iNOS protein in a dose-dependent manner (Figure 1D), which was further supported by the immunostaining results (Figure 1E, F). Next, we evaluated whether TPX inhibited LPS-stimulated elevation of pro-inflammatory cytokines in RAW264.7 cells. The ELISA results showed that TPX significantly suppressed the levels of IL-6 and TNF-α in LPS-stimulated macrophages (Figure 1G, H). Furthermore, real-time RT-PCR results showed that the mRNA levels of IL-6, TNF-α and IL-1β were markedly reduced by TPX treatment, compared with those of LPS treatment alone (Figure 1I–K). The mRNA and protein levels of COX-2 were increased after LPS treatment, and TPX significantly blocked this increase in COX-2 (Supporting Information Figure S3A, B). Taken together, the above data indicate that TPX suppresses LPS-stimulated inflammatory responses in macrophages.

TPX suppresses LPS-induced inflammation in macrophages through the MAPKs and NF-κB pathways

MAPKs and NF-κB signalling pathways are key regulators of inflammation (Qian *et al.,* 2015). As expected, LPS treatment

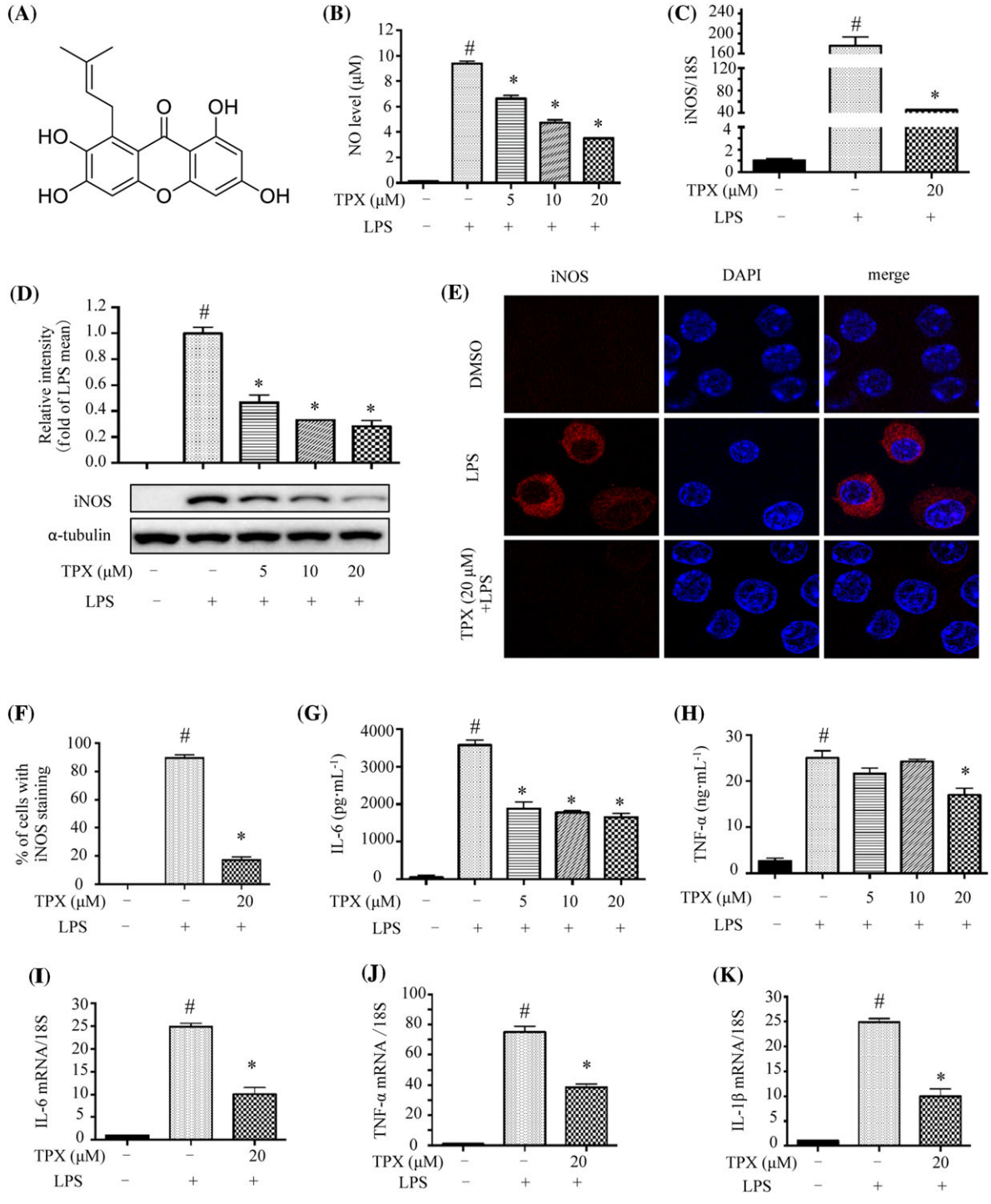

Figure 1

TPX suppressed inflammatory responses in LPS-treated RAW264.7 macrophages. (A) Chemical structure of TPX. (B) Cells were treated with TPX at different concentrations range from 5 to 20 μM in the presence of LPS (1 μg·mL^{-1}) for 18 h. NO production was determined by Griess reagent (n = 9). Cells were pretreated with vehicle or TPX (20 μM) for 1 h, followed by treatment with LPS (1 μg·mL^{-1}) for 6 h. (C) The mRNA level of iNOS was analysed by real-time RT-PCR, normalized to 18S (n = 6). (D) The expression of iNOS protein was determined by Western blotting (n = 5). α-Tubulin was used as an internal loading control. Data were normalized to the mean value of the LPS group. (E) The immunostaining of iNOS in the different groups. Nuclei were stained with DAPI. (F) The percentage of iNOS positive cells was evaluated from the immunostaining images (n = 5). Cells were pretreated with different concentrations of TPX for 1 h and then stimulated with LPS (1 μg·mL^{-1}) for 18 h. The levels of IL-6 (G) and TNF-α (H) were determined by ELISA kits (n = 6). Cells were pretreated with TPX (20 μM) for 1 h and then stimulated with LPS (1 μg·mL^{-1}) for 6 h. The mRNA levels of IL-6 (I), TNF-α (J) and IL-1β (K) were analysed by real-time RT-PCR, and normalized to 18S (n = 6). Data are expressed as means ± SEM. $^{\#}P < 0.05$ versus DMSO, $^{*}P < 0.05$ versus LPS.

increased the phosphorylation of p38, JNK and ERK; remarkably, TPX blocked the phosphorylation of p38, JNK and ERK (Figure 2A). With regard to the NF-κB pathway, the phosphorylation of IKKα/β, IκBα and p65 were increased remarkably by LPS stimulation, and these effects were reversed by TPX treatment (Figure 2B). Since the nuclear translocation of the NF-κB transcriptional subunit p65 is a critical step for the activation of the NF-κB signalling pathway, we then investigated whether TPX affected the subcellular compartmentalization of p65. The confocal microscopic analysis revealed a greater proportion of p65 translocated to the nucleus in LPS-stimulated RAW264.7 cells; while pretreatment with TPX significantly reduced this nuclear accumulation of p65 (Figure 2C, D). The Western blot analysis further confirmed the above result (Figure 2E, F). The NF-κB luciferase reporter assay further confirmed that the NF-κB transcriptional activity was inhibited by TPX treatment compared to LPS treatment alone (Figure 2G). These results demonstrate that TPX suppresses the activation of the MAPKs and NF-κB signalling pathways.

TPX suppresses LPS-induced inflammation through activating SIRT3

SIRT3 has been reported to modulate the activation of the MAPKs and NF-κB signalling pathways in an inflammatory model (Koyama *et al.,* 2011). We found that LPS treatment decreased the expression of SIRT3 protein compared to vehicle control, and TPX significantly increased SIRT3 expression in LPS-treated macrophages (Figure 3A). To further verify that the anti-inflammatory effect of TPX is mediated through SIRT3, a SIRT3 silenced RAW264.7 cell line (SIRT3 silence) was generated using shRNA targeting SIRT3. The SIRT3 silence cell line expressed about 50% less SIRT3 protein compared with that of the cells expressing scrambled shRNA (scrambled) (Figure 3B). LPS induced a significantly higher level of NO and iNOS expression in SIRT3-silenced cells compared with those in scrambled cells (Figure 3C, D). Additionally, SIRT3-silenced cells expressed higher level of IL-6 (Figure 3E). In contrast, the anti-inflammatory activity of TPX was partially blocked in LPS-induced SIRT3-silenced cells (Figure 3C–G). These data indicate that SIRT3, at least partially, mediates the anti-inflammatory effect of TPX in LPS-stimulated macrophages.

TPX prevents TNF-α-induced inflammation in adipocytes through an effect on the MAPKs and NF-κB signalling pathways

TNF-α produced by macrophages plays a critical role in the induction of inflammation in adipocytes (Watanabe *et al.,* 2016). Phosphorylated JNK, ERK and p38 levels were elevated in TNF-α-stimulated 3T3-L1 adipocytes, and TPX significantly reversed the activation of JNK, ERK and p38 (Figure 4A). Phosphorylation and degradation of NF-κB signals were observed in TNF-α-stimulated 3T3-L1 adipocytes (Figure 4B). TPX strongly inhibited TNF-α-induced phosphorylation of IκBα, p65 and IKKα/β compared to adipocytes only treated with TNF-α (Figure 4B). Moreover, TPX significantly increased SIRT3 protein expression in TNF-α-treated adipocytes (Figure 4C). Thus, TPX alleviates TNF-α mediated inflammation in adipocytes, presumably through promoting the expression of SIRT3 and inhibiting the activation of the NF-κB and MAPKs pathways.

TPX prevents the migration of macrophages to adipocytes in vitro

To examine the functional consequences of the inhibitory effect of TPX on adipocyte inflammation, macrophage migration experiments were performed using co-cultures of 3T3-L1 adipocytes and RAW264.7 macrophages (Karkeni *et al.,* 2015). RAW264.7 macrophages were seeded into the upper insert well of the chemotaxis chamber and incubated in the presence of DMEM or adipocyte CM in the lower chamber (Figure 5A, B). Adipocyte CM significantly induced macrophage chemotaxis in comparison to DMEM, and a more pronounced effect was observed with CM plus TNF-α (Figure 5A). However, macrophage migration was suppressed when the cells were exposed to the CM from adipocytes treated with TNF-α and TPX (Figure 5A; Supporting Information Figure S4A), indicating that TPX might inhibit the TNF-α-induced expression of chemoattractants in adipocytes. Furthermore, pretreatment of the macrophages with TPX also prevented their migration to adipocyte CM (Figure 4B; Supporting Information Figure S4B). To confirm that TPX modulates LPS-mediated chemokine expression in macrophages, the mRNA levels of chemokines were assessed. As expected, LPS treatment significantly increased the level of MCP-1 and the mRNA expression levels of MCP-1, MIP-1α, C-X-C motif chemokine 10 (***Cxcl10***), chemokine (C-C motif) ligand 11 (***Ccl11***) and **chemokine** (C-X3-C motif) ligand 1(*Cx3cl1*), whereas TPX significantly decreased the expressions of these chemokines compared with LPS-treated alone (Figure 5C–H). These results indicate that TPX interferes with macrophage chemotaxis when either macrophages or adipocytes are exposed to TPX.

TPX treatment attenuates LPS-mediated inflammatory responses in epididymal adipose tissue

To examine the effects of TPX on inflammatory responses in adipose tissue *in vivo*, a mouse model of LPS-induced acute inflammation was implemented (Figure 6A). TPX treatment had no effect on the body weights of the mice (Supporting Information Figure S5). As shown in Figure 6B–D, a significant increase of TNF-α, IL-6 and MCP-1 levels in serum was observed after LPS treatment, whereas 5 day TPX administration significantly reduced the cytokine levels in these LPS-treated mice. Consistently, TPX ameliorated LPS-induced increase in cytokines in epididymal adipose tissue, as assessed by ELISA kits (Figure 6E–G) and real-time RT-PCR (Figure 6H–M).

To assess the underlying mechanisms, real-time RT-PCR was performed to evaluate the mRNA expressions of chemokines and macrophage markers in epididymal adipose tissue. The mRNA levels of chemokines including MCP-1, MIP-1α, CXCL10, CCl11 and **CCL5** were significantly elevated in LPS-treated adipose tissue, and pretreatment with TPX strongly suppressed the expression levels (Figure 7A–E), which indicated TPX could prevent LPS-induced macrophage infiltration into adipose tissue. The mRNA levels of, F4/80 and CD68 were significantly elevated in LPS-treated adipose

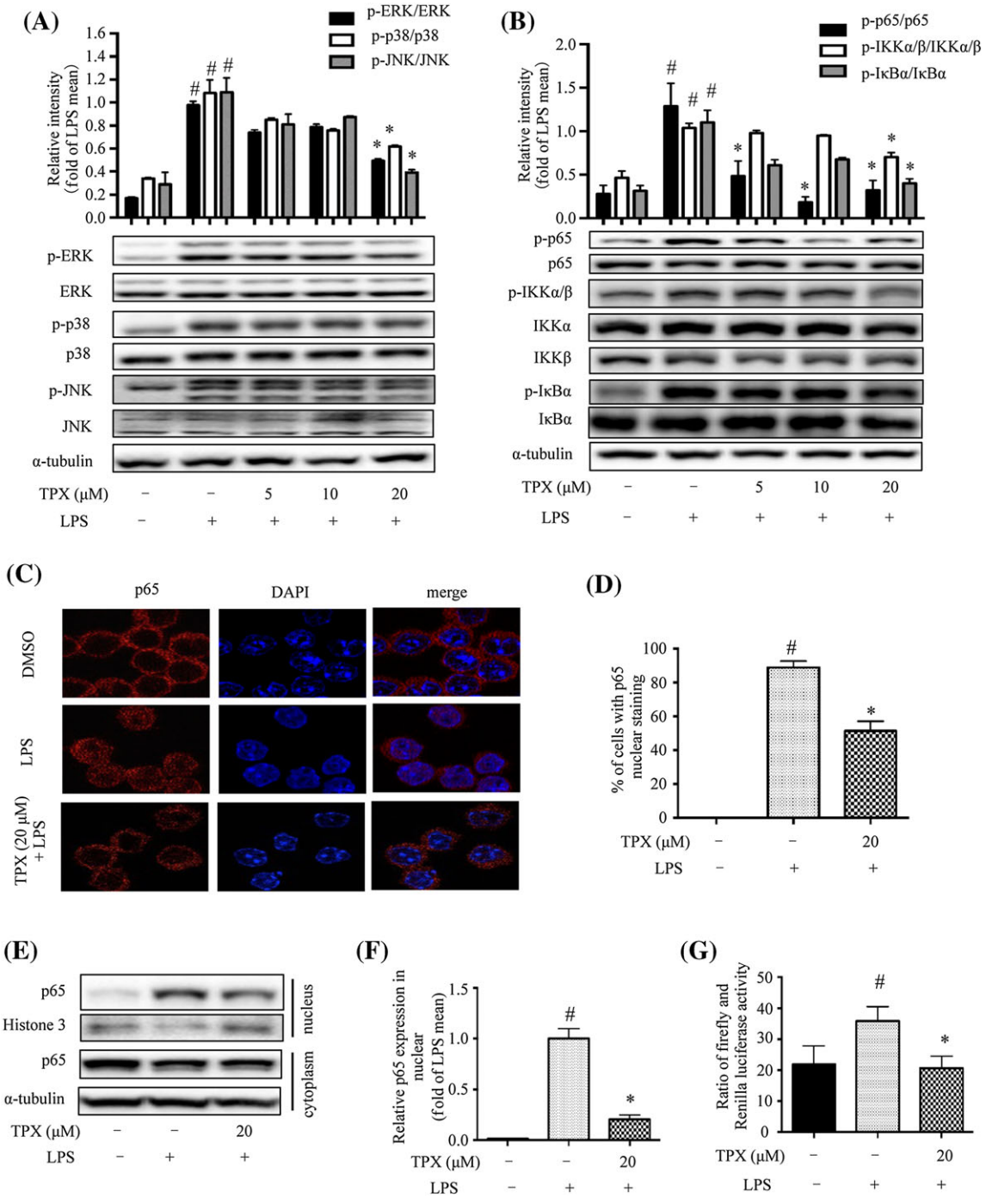

Figure 2

TPX blocked MAPK phosphorylation and inhibited NF-κB activity in LPS-treated RAW264.7 macrophages. Cells were treated with TPX in the absence or presence of LPS (1 μg·mL^{-1}) for the indicated time. (A) The protein levels of phospho-ERK, ERK, phospho-p38, p38, phospho-JNK and JNK were detected by Western blot analyses (n = 6). α-Tubulin was used as internal loading control. Data were normalized to the mean value of the LPS group. (B) The protein levels of phospho-IKKα/β, IKKα, IKKβ, phospho-IκBα, IκBα, phospho-p65 and p65 were detected by Western blot analyses (n = 6). α-Tubulin was used as internal loading control. Data were normalized to the mean value of the LPS group. (C) Cells were pretreated with or without TPX (20 μM) for 1 h and then exposed to LPS (1 μg·mL^{-1}) for another 1 h. The immunostaining of p65 was detected. Nuclei were stained with DAPI. (D) The percentage of cells undergoing p65 nuclear translocation was quantified (n = 6). (E) The protein level of p65 in nuclear and cytoplasmic fractions was determined by Western blotting. Histone 3 and α-tubulin were used as internal loading controls. (F) The relative expression of p65 in the nuclear fraction was quantified (n = 6). Data are normalized to the mean value of LPS group. (G) RAW264.7 cells were co-transfected with a NF-kB luciferase reporter gene and pRL Renilla luciferase control reporter vector, then the cells were pretreated with TPX for 1 h followed by activation with LPS for 1 h. The transcriptional activity was expressed as the ratio of firefly to Renilla luciferase intensities in the cell lysates (n = 6). Data are expressed as means ± SEM. $^{\#}P < 0.05$ versus DMSO, $^{*}P < 0.05$ versus LPS.

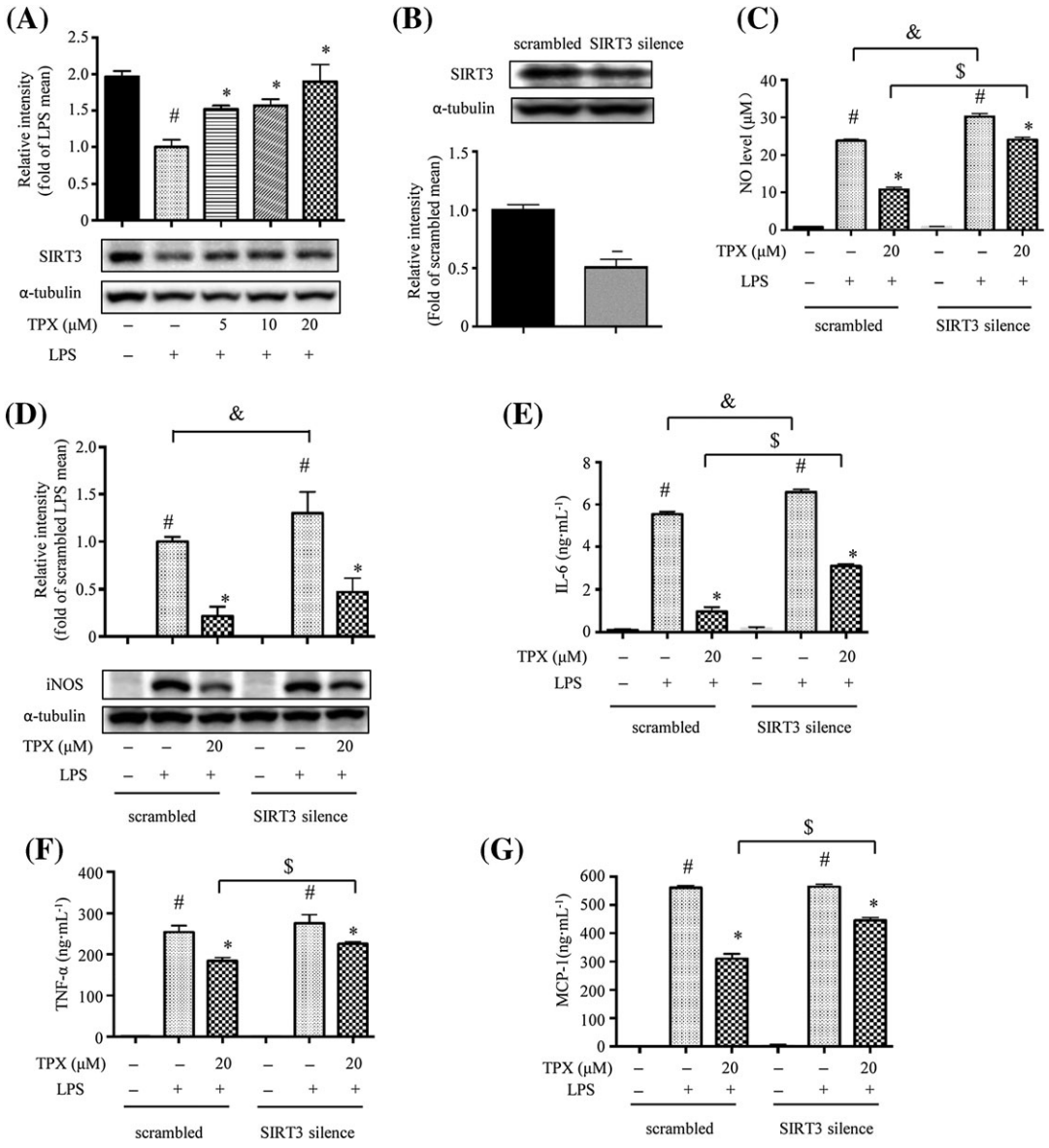

Figure 3

The anti-inflammatory effect of TPX in RAW264.7 macrophages is partially mediated through SIRT3. (A) The protein expression of SIRT3 was determined by Western blotting ($n = 6$). α-Tubulin was used as an internal loading control. Data were normalized to the mean value of the LPS group. (B) SIRT3 expression in SIRT3 silenced RAW264.7 macrophages (SIRT3 silence) and control cells (scrambled) was determined by Western blotting ($n = 6$). α-Tubulin was used as an internal loading control. Data were normalized to the mean value of scrambled group. (C) Cells were treated with 20 μM TPX in the presence of LPS (1 μg·mL^{-1}) for 18 h. NO production was determined by Griess reagent ($n = 6$). (D) iNOS abundance was measured by Western blotting ($n = 6$). Data were normalized to the mean value of the scrambled LPS group. Cells were pretreated with TPX for 1 h and then stimulated with LPS (1 μg·mL^{-1}) for 18 h. The levels of IL-6 (E), TNF-α (F) and MCP-1 (G) were determined by ELISA kits ($n = 6$). Data are expressed as means ± SEM. $^{\#}P < 0.05$ versus DMSO, $^{*}P < 0.05$ versus LPS, $^{\&}P < 0.05$ versus scrambled LPS, $^{\$}P < 0.05$ versus scrambled TPX.

tissue, and pretreatment with TPX obviously suppressed the expression levels (Figure 7F–H), which further indicated TPX prevents LPS-induced macrophage accumulation in adipose tissue. Interestingly, TPX treatment suppressed the expression of the M1 macrophage marker CD11c (Figure 7I), while elevated expressions of the M2 macrophage markers ARG1 and CD206 (Figure 7J, K), which suggested TPX promotes a shift in macrophages towards an anti-inflammatory M2 phenotype.

As shown in Figure 8A, the iNOS expression was increased after LPS injection, and TPX reduced the iNOS level in epididymal adipose tissue. SIRT3 expression was markedly reduced after LPS injection in epididymal adipose tissue, and TPX significantly reversed this decrease in SIRT3 (Figure 8A). Regarding the MAPKs pathway, the phosphorylation of p38 and ERK was increased following LPS injection, and TPX significantly blocked the phosphorylation of p38 and ERK (Figure 8B). Compared to the control group, the phosphorylation of

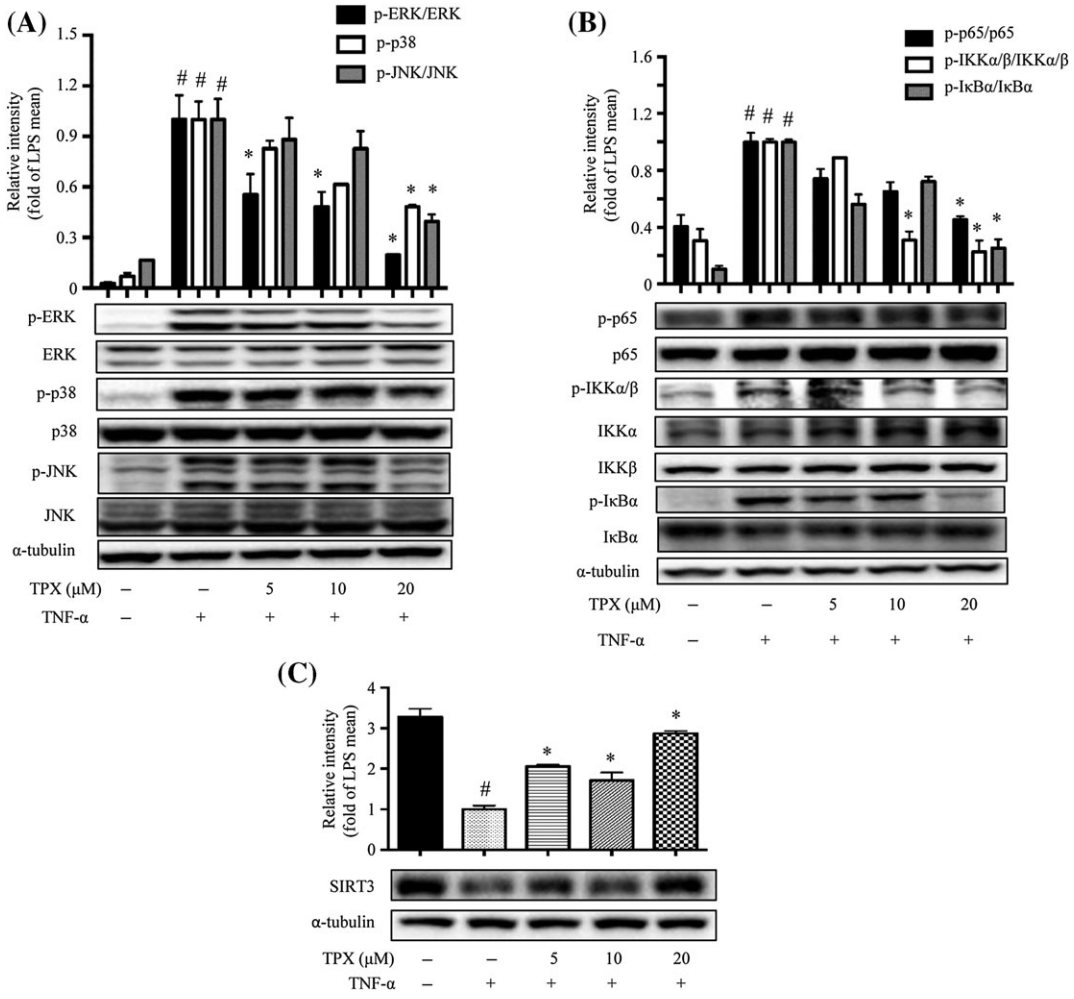

Figure 4

TPX prevented TNF-α-induced inflammatory changes in adipocytes. Differentiated 3T3-L1 adipocytes were treated with TPX for 6 h and subsequently stimulated with TNF-α (15 ng·mL^{-1}). (A) The protein levels of phospho-ERK, ERK, phospho-p38, p38, phospho-JNK and JNK were detected by Western blot analyses (n = 6). α-Tubulin was used as an internal loading control. Data were normalized to the mean value of the TNF-α group. (B) The protein levels of phospho-IKKα/β, IKKα, IKKβ, phospho-IκBα, IκBα, phospho-p65 and p65 were detected by Western blot analyses (n = 6). α-Tubulin was used as an internal loading control. Data were normalized to the mean value of the TNF-α group. (C) The protein expression of SIRT3 was determined by Western blotting, and α-tubulin was used as an internal loading control (n = 6). Data were normalized to the mean value of the TNF-α group. Data are expressed as means ± SEM. $^{\#}P < 0.05$ versus DMSO, $^{*}P < 0.05$ versus TNF-α.

IKKα/β, IκBα and p65 was increased markedly by LPS stimulation, while being significantly suppressed by the TPX treatment (Figure 8C). These data demonstrated that TPX prevents LPS-induced inflammatory responses in adipose tissue through increasing SIRT3 expression and blocking the activation of the NF-κB and MAPKs signalling pathways.

Discussion

Obesity is associated with chronic inflammation in adipose tissue. There is a clear correlation between the onset of insulin resistance and type 2 diabetes and macrophage infiltration into adipose tissue and pro-inflammatory cytokine secretion from adipose tissue. Anti-inflammatory therapies have been proved to improve insulin sensitivity in animals (Yuan *et al.*, 2001; Lin *et al.*, 2016). NO is a mediator and regulator of inflammatory responses, and is mainly produced in macrophages by iNOS (Qian *et al.*, 2015). IL-6 is a multifunctional cytokine produced by different cell types and is an important autocrine and paracrine regulator of adipose tissue metabolism (Mohamed-Ali *et al.*, 1997). Currently, several xanthones have been found to show inhibitory effects on either NO production or IL-6 secretion. TPX was the only one active in both assays, which suggests that it has potential as an anti-inflammatory molecule. Moreover, TPX was verified to suppress inflammatory responses in adipose tissue *in vivo*. The anti-inflammatory activity of xanthones from *G. mangostana* was observed previously; β-mangostin was reported to suppress carrageenan-induced peritonitis (Syam *et al.*, 2014) and α-mangostin attenuated brain inflammation in peripheral LPS-treated mice (Catorce *et al.*, 2016). However, the results of this study are the first to show a direct effect of a xanthone on adipose tissue inflammation.

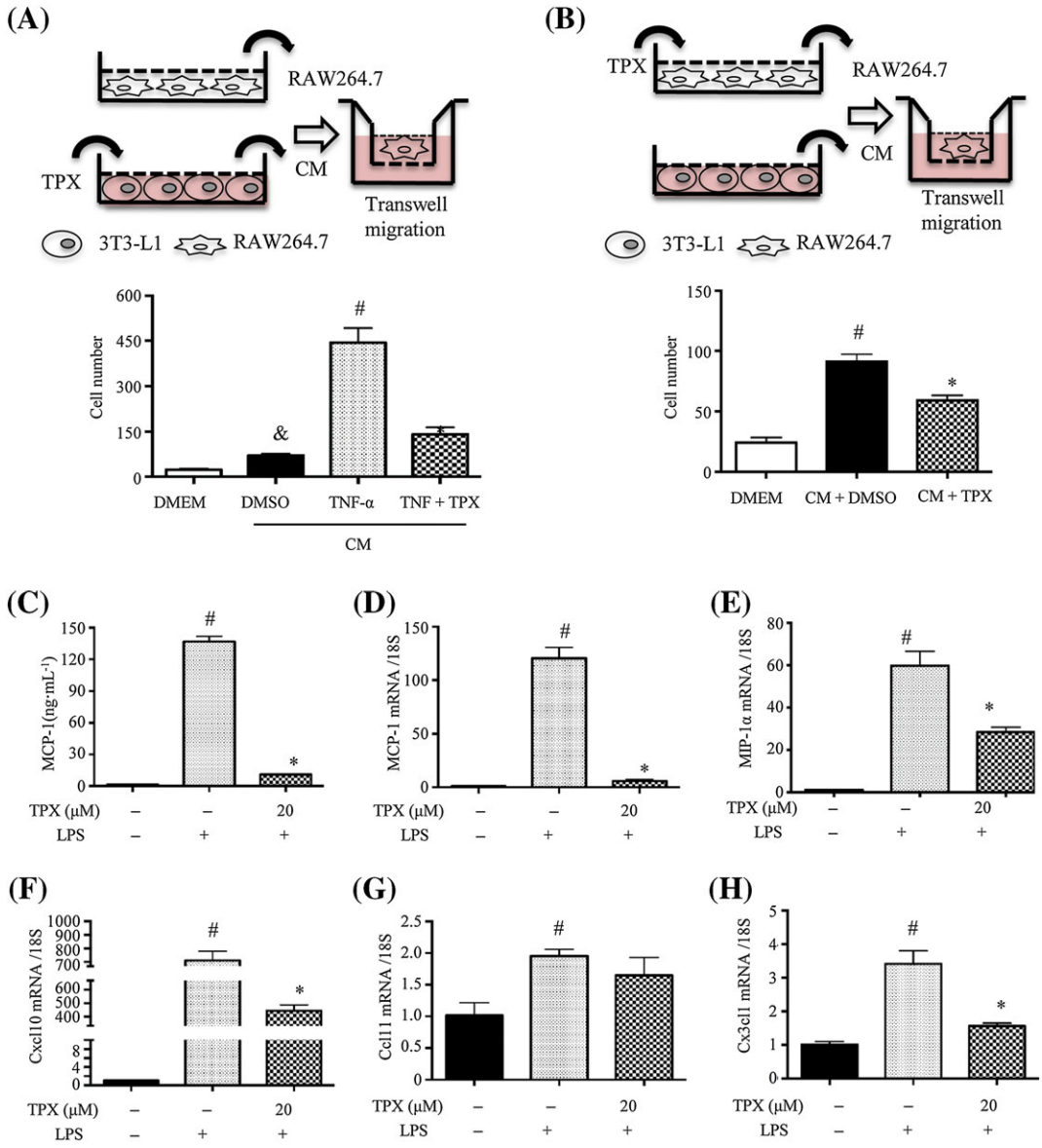

Figure 5

TPX decreased the migration of RAW264.7 macrophages towards 3T3-L1 adipocytes. (A, B) Procedures of the macrophage migration experiments. (A) Macrophage migration assays using DMEM (migration media) or CM from adipocytes treated with vehicle, TNF-α (15 ng·mL^{-1}) or TNF-α (15 ng·mL^{-1}) + TPX (20 μM) for 24 h. Migrated RAW264.7 macrophages were visualized by DAPI staining and quantified (n = 6). (B) RAW264.7 cells were treated with vehicle or TPX (20 μM) for 4 h, and the detached cells were used for the migration assay in the presence of DMEM or CM. Migrated RAW264.7 macrophages were visualized by DAPI staining and quantified (n = 6). (C) Cells were pretreated with TPX for 1 h and then stimulated with LPS (1 μg·mL^{-1}) for 18 h. The levels of MCP-1 were determined by an ELISA kit (n = 6). RAW264.7 macrophages were pretreated with TPX (20 μM) for 1 h and then stimulated with LPS (1 μg·mL^{-1}) for 6 h. The mRNA levels of MCP-1 (D), MIP-1α (E), Cxcl10 (F), Ccl11 (G) and Cx3cl1 (H) were analysed by real-time RT-PCR, and normalized to 18S (n = 6). Data are expressed as means ± SEM, $^{\#}P < 0.05$ versus DMSO, $^{*}P < 0.05$ versus LPS, $^{\&}P < 0.05$ versus DMEM.

The bioavailability and metabolism of xanthones, especially α-mangostin, have been investigated in rodents and humans (Gutierrez-Orozco and Failla, 2013). The bioavailability of α-mangostin was low when administered p.o. but relatively high when injected i.p. or i.v. The concentration of α-mangostin in fat tissue was 0.0391 ± 0.0825 μg·g^{-1} 150 min after an i.v. injection of 5 mg·kg^{-1} in mice (Choi *et al.*, 2014). The median lethal dosage of α-mangostin after i.p. administration was 150.0 mg·kg^{-1}, which was mainly metabolized *via* liver and small intestine by phase II reaction such as glucuronide and sulfate conjugations (Bumrungpert *et al.*, 2009). Until now, the bioaccessibility and metabolism of TPX had not been investigated. In our preliminary study, an i.p. injection of a high dose of TPX (40 mg·kg^{-1}) caused severe diarrhoea in mice. Thus, the dose of TPX used in our *in vivo* study was set at 20 mg·kg^{-1}.

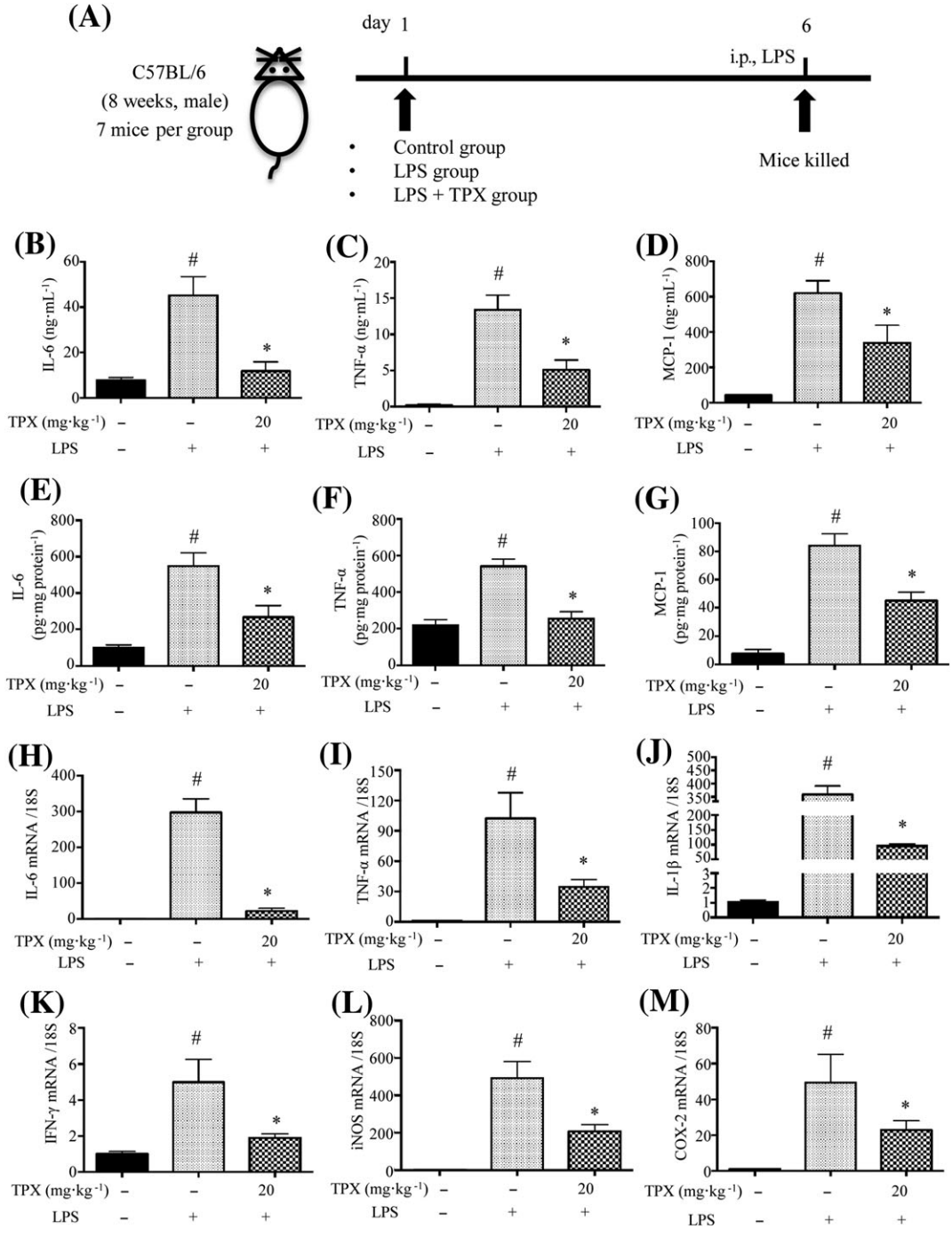

Figure 6

TPX ameliorates LPS-mediated inflammatory responses in epididymal adipose tissue of mice. (A) The procedure used to produce the mouse model of LPS-mediated acute inflammation. The serum levels of IL-6 (B), TNF-α (C) and MCP-1 (D) were determined by ELISA kits. The epididymal adipose tissue levels of IL-6 (E), TNF-α (F) and MCP-1 (G) were determined by ELISA kits. (H–M) Results of real-time RT-PCR analyses of pro-inflammatory cytokines expression in epididymal adipose tissue. Data are expressed as means ± SEM ($n = 7$). $^{\#}P < 0.05$ versus DMSO, $^{*}P < 0.05$ versus LPS.

NF-κB is a primary regulator of inflammatory responses in a variety of physiological and pathological processes (Suganami *et al.*, 2007). NF-κB dimers are located in cytosol under normal conditions, combined with its inhibitor protein IκBα (Fan *et al.*, 2015). In response to inflammatory stimuli, NF-κB is activated through the phosphorylation and subsequent degradation of IκBα by IKK complex (Joo *et al.*, 2009). The activated NF-κB dimer dissociates from IκBα and subsequently translocates to the nucleus, where it induces the expression of various inflammatory genes (Soromou *et al.*, 2012). In the present study, TPX was found to suppress LPS-induced activation of IKKα/β, IκBα and p65, prevent the

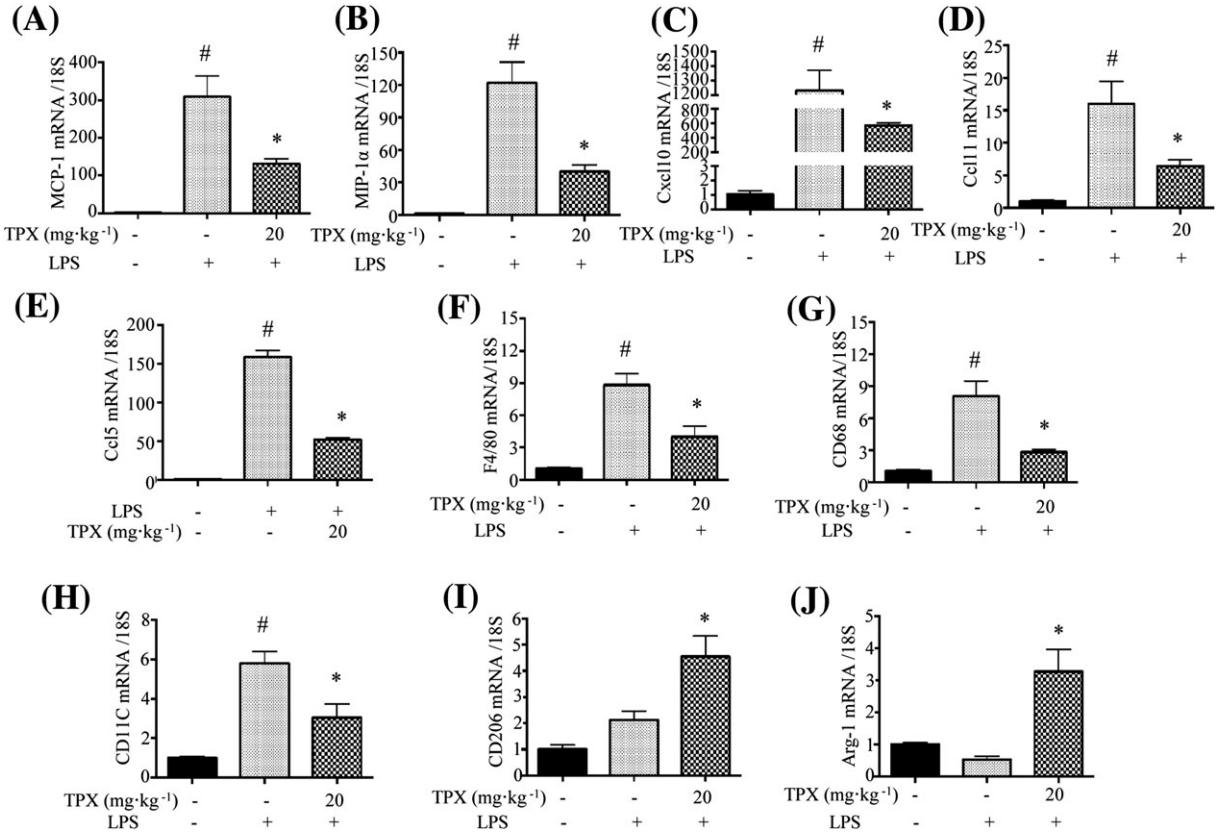

Figure 7

Effect of TPX on the expressions of chemokines and macrophage markers in epididymal adipose tissue. Results of real-time RT-PCR analyses for pro-inflammatory chemokines in epididymal adipose tissue, including MCP-1 (A), MIP-1α (B), Cxcl10 (C), Ccl11 (D) and Ccl5 (E). Real-time RT-PCR analyses for macrophage markers in epididymal adipose tissue are also shown, including F4/80 (F), CD68 (G), CD11c (H), CD206 (I) and Arg-1 (ARG1; J). Data are expressed as means ± SEM ($n = 7$). $^{\#}P < 0.05$ versus DMSO, $^{*}P < 0.05$ versus LPS.

translocation of NF-κB/p65 from cytoplasm to nucleus and inhibit NF-κB transcriptional activity in macrophages, resulting in a reduction in its downstream genes including iNOS, COX-2 and TNF-α. These data suggested that xanthones might be a new class of inhibitors of the NF-κB signalling pathway. Low-level NF-κB activation has been identified in adipose tissue, which shares a similar time course of activation as immune cells (McArdle *et al.*, 2013). In adipocytes, TNF-α activates the NF-κB signalling pathway to induce lipolysis, stimulate cytokine expression and promote insulin resistance (Wellen and Hotamisligil, 2003). TPX significantly inhibited TNF-α-induced activation of the NF-κB signalling pathway in adipocytes. MAPKs are a large family of seine/threonine kinases that mediate the inflammatory signalling upon extracellular stimulation, and include ERK, p38 and JNK (Qian *et al.*, 2015). These cytoplasmic enzymes can phosphorylate and activate various transcription factors in the cytoplasm or nucleus (Hommes *et al.*, 2003). TPX suppressed the phosphorylation of ERK, p38 and JNK in LPS-stimulated macrophages, TNF-α-stimulated adipocytes and LPS-treated mice. These finding suggested that TPX might suppress inflammatory responses in macrophages and adipocytes through an effect on the NF-κB and MAPK signalling pathways, to attenuate adipose tissue inflammation.

Activators of the PPARs have been shown to exert anti-inflammatory activity in various cells by inhibiting the expression of pro-inflammatory genes such as cytokines, metalloproteases and acute-phase proteins (Delerive *et al.*, 2001). The transcriptional factors NF-κB and activator protein 1 are known to be downstream components of PPARβ signalling and are critical for LPS-mediated gene induction (Xu *et al.*, 2013). PPARβ activation inhibited LPS-induced MAPK and NF-κB activation (Planavila *et al.*, 2005; Xu *et al.*, 2013). We found that PPARs expressions were rapidly down-regulated after stimulation with LPS, and TPX treatment significantly promoted PPARα and PPARβ expressions in LPS-treated macrophages (Supporting Information Figure S6), which suggests that the anti-inflammatory and M2 macrophage polarizing effects of TPX might be mediated through PPARs.

A deficiency in SIRT3 and the accompanying mitochondrial protein hyperacetylation were reported to be associated with the development of metabolic syndrome and hepatocyte injury (Chang *et al.*, 2016; Liu *et al.*, 2017). RAW264.7 macrophages with SIRT3 knockdown expressed higher iNOS protein and transcript levels of inflammatory cytokines, which led to an elevated inflammatory state (Xu *et al.*, 2016). SIRT3 has been reported to suppress MAPK activation

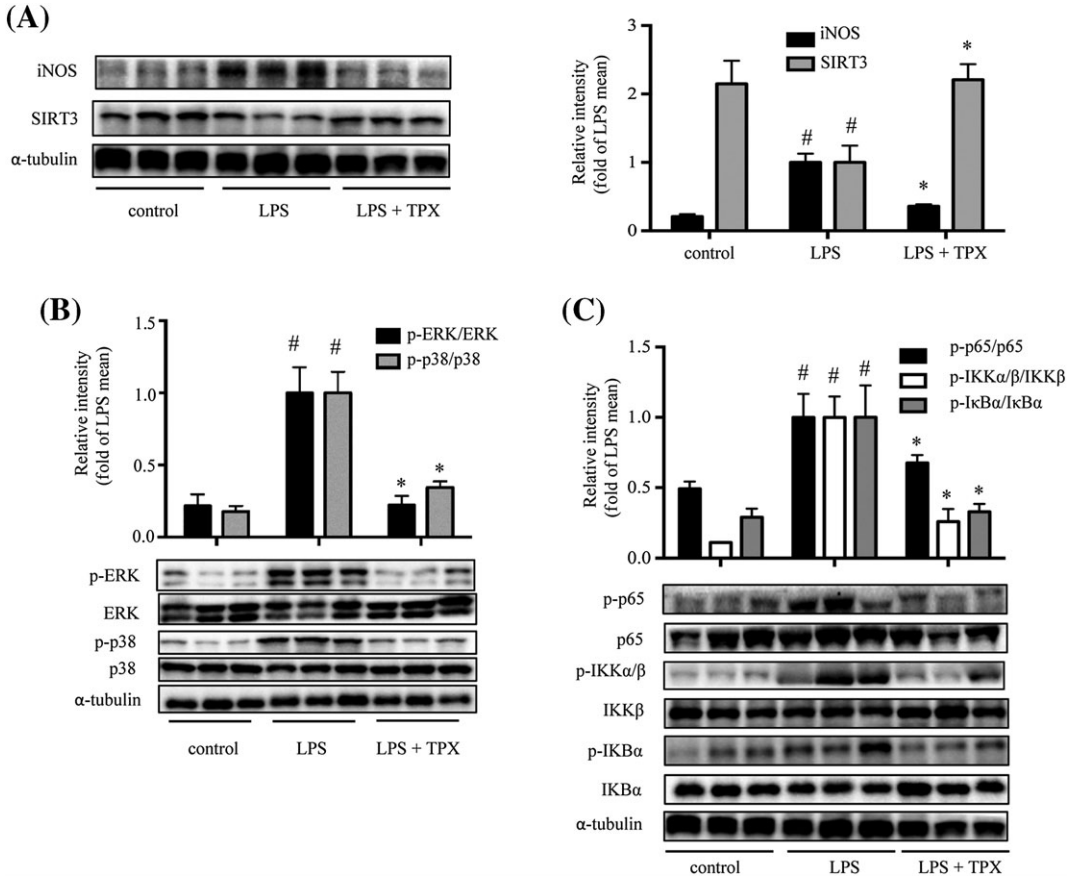

Figure 8

TPX inhibited LPS-mediated MAPK phosphorylation and NF-κB activity in epididymal adipose tissue. (A) The protein levels of iNOS and SIRT3 in adipose tissue were detected by Western blot analyses. α-Tubulin was used as an internal loading control. Data were normalized to the mean value of the LPS group. (B) The protein levels of phospho-ERK, ERK, phospho-p38 and p38 were detected by Western blot analyses. GAPDH was used as an internal loading control. Data were normalized to the mean value of the LPS group. (C) The protein levels of phospho-IKKα/β, IKKβ, phospho-IκBα, IκBα, phospho-p65 and p65 were detected by Western blot analyses. α-Tubulin was used as an internal loading control. Data were normalized to the mean value of LPS group. Data are expressed as means ± SEM ($n = 7$). $^{\#}P < 0.05$ versus DMSO, $^{*}P < 0.05$ versus LPS.

in various models of inflammation (Sundaresan *et al.*, 2009; Kim *et al.*, 2015). Overexpression of SIRT3 in H9c2 cells inhibited NF-κB nuclear translocation, which stimulated SOD2 gene expression and consequently conferred cells with resistance against oxidative insults (Chen *et al.*, 2013). Consistently, our data showed that the SIRT3 level was decreased in LPS-treated macrophages and TNF-α-treated adipocytes, as well as in adipose tissue from LPS-treated mice, which corroborates that SIRT3 represents an inflammatory target protein. Interestingly, TPX significantly increased SIRT3 expression in LPS-treated macrophages, TNF-α-stimulated adipocytes and LPS-treated mice, but not SIRT1 (data not shown). SIRT3, at least partially, mediates the inhibitory effect of TPX on inflammatory responses in macrophages. Further studies are needed to determine how TPX regulates SIRT3 expression.

Inflammatory chemokines are the main participants in the recruitment and activation of circulating monocytes in inflammatory responses (Mantovani *et al.*, 2004). MCP-1 and MIP-1α, known to possess strong chemoattractant activity, are produced predominantly by macrophages and endothelial cells (Kanda *et al.*, 2006). MCP-1 is a potential stimulus for macrophage proliferation in obese adipose tissue, which contributes to obesity-associated adipose tissue inflammation (Amano *et al.*, 2014). MIP-1α, involved in the acute inflammatory state in the recruitment and activation of polymorphonuclear leukocytes, is robustly up-regulated in white adipose tissue of obese mice and infiltrated macrophages secrete MIP-1α in inflamed fat (Zhuge *et al.*, 2016). In adipose tissue, both adipocytes and the infiltrated immune cells are responsible for secretion of MCP-1. The secretion of MCP-1 from adipocytes directly triggers the recruitment of macrophages to adipose tissue, and the infiltrated macrophages may in turn secrete a variety of chemokines and other cytokines that further promote a local inflammatory response and affect gene expression in adipocytes, resulting in systemic insulin resistance (Kanda *et al.*, 2006). Here, we found that MCP-1, MIP-1α, *Cxcl10*, *Ccl11* and *Ccl5* levels were elevated in LPS-stimulated macrophages and adipose tissue, and TPX reversed these increases in chemokine levels. It is proposed that the reduced number of macrophages in adipose tissue of TPX-treated mice is likely through TPX blocking their infiltration from the circulation and inhibiting their local proliferation. An *in vitro* chemotaxis assay with adipocyte CM was conducted to assess the ability of

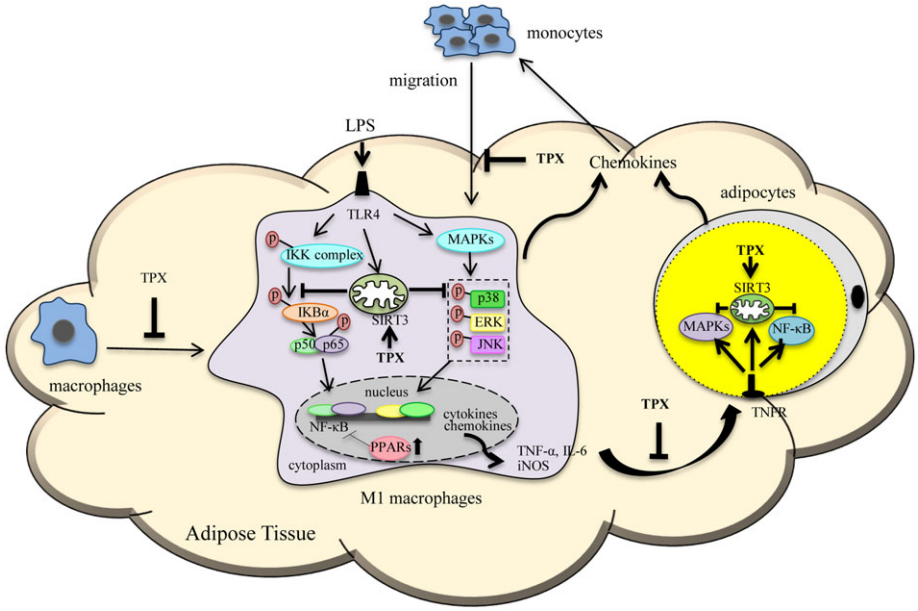

Figure 9

Schematic models of molecular targets affected by TPX to attenuate inflammatory signalling pathways.

macrophages to migrate towards adipocytes. Our results showed that the CM from TPX-treated adipocytes inhibited macrophage migration, and that the chemotactic ability towards CM from differentiated adipocytes was impaired in TPX-treated macrophages. In a previous study it was demonstrated that chemokines induce macrophage migration to adipose tissue *via* MAPKs signalling (Wang *et al.*, 2014). It was supposed TPX impairs chemokines-induced migration of macrophages through inhibiting NF-κB and MAPK activation and promoting SIRT3 expression.

Activated, infiltrated macrophages are a prominent source of pro-inflammatory cytokines, which block insulin action in adipose tissue and subsequently cause systemic insulin resistance. Therefore, preventing the infiltration of macrophages into adipose tissue could ameliorate obesity-linked inflammation and insulin resistance, providing a therapeutic target for metabolic syndrome. Indeed, macrophage numbers and pro-inflammatory cytokine levels in intra-abdominal adipose tissue were increased in LPS-treated mice. Remarkably, TPX treatment decreased pro-inflammatory cytokine levels in serum and epididymal adipose tissue and significantly reduced the expression of the macrophage markers F4/80 and CD68 in LPS-treated mice, which indicates that TPX reduced macrophage accumulation in adipose tissue after LPS stimulation. Furthermore, TPX treatment suppressed the expressions of M1 macrophage marker CD11c, while elevating those of the M2 macrophages, including ARG1 and CD206, suggesting a shift towards an anti-inflammatory phenotype. However, further studies are needed to determine the anti-inflammatory effect of TPX in diet-induced obese animals, such a Western diet-fed mice and/or genetically obese animals, such as *ob/ob* mice. Moreover, adipose tissue inflammation is associated with insulin resistance; and the effect of TPX on energy homeostasis and insulin sensitivity should be evaluated using obese animal models.

In conclusion, TPX, a xanthone derived from *G. mangostana*, was shown to have anti-inflammatory effects in LPS-treated macrophages and TNF-α-treated adipocytes *in vitro* and these effects were further authenticated in a murine model of LPS-induced acute inflammation *in vivo*. TPX ameliorates inflammatory responses in macrophages and adipocytes, possibly through inhibiting NF-κB and MAPK signalling pathways (Figure 9). The current results demonstrate that TPX is involved in preventing macrophage accumulation and promoting a macrophage shift toward an anti-inflammatory phenotype in adipose tissue. TPX could be a candidate for treating adipose tissue inflammation and related metabolic disorders and warrants further investigation.

Acknowledgements

Financial support by Science and Technology Development Fund, Macao S.A.R (FDCT 120/2013/A3) and the Research Fund of University of Macau (MYRG2015-00153-ICMS-QRCM and MYRG2017-00109-ICMS) are gratefully acknowledged.

Author contributions

D.L., Q.L. and W.S. conducted research and analysed data; D.L. and L.L. designed the experiments and wrote the paper; X.C., Y.W. and Y.S. consulted for the study and proofread the paper. L.L. conceived the study.

Conflict of interest

The authors declare no conflicts of interest.

Declaration of transparency and scientific rigour

This Declaration acknowledges that this paper adheres to the principles for transparent reporting and scientific rigour of preclinical research recommended by funding agencies, publishers and other organisations engaged with supporting research.

References

Alexander SPH, Cidlowski JA, Kelly E, Marrion NV, Peters JA, Faccenda E *et al*. (2017a). The Concise Guide to PHARMACOLOGY 2017/18: Nuclear hormone receptors. Br J Pharmacol 174: S208–S224.

Alexander SPH, Fabbro D, Kelly E, Marrion NV, Peters JA, Faccenda E *et al*. (2017b). The Concise Guide to PHARMACOLOGY 2017/2018: Enzymes. Br J Pharmacol 174: S272–S359.

Amano SU, Cohen JL, Vangala P, Tencerova M, Nicoloro SM, Yawe JC *et al*. (2014). Local proliferation of macrophages contributes to obesity-associated adipose tissue inflammation. Cell Metab 19: 162–171.

Bensinger SJ, Tontonoz P (2008). Integration of metabolism and inflammation by lipid-activated nuclear receptors. Nature 454: 470–477.

Bumrungpert A, Kalpravidh RW, Suksamrarn S, Chaivisuthangkura A, Chitchumroonchokchai C, Failla ML (2009). Bioaccessibility, biotransformation, and transport of alpha-mangostin from *Garcinia mangostana* (Mangosteen) using simulated digestion and Caco-2 human intestinal cells. Mol Nutr Food Res 53 (Suppl 1): S54–S61.

Catorce MN, Acero G, Pedraza-Chaverri J, Fragoso G, Govezensky T, Gevorkian G (2016). Alpha-mangostin attenuates brain inflammation induced by peripheral lipopolysaccharide administration in C57BL/6J mice. J Neuroimmunol 297: 20–27.

Chae HS, You BH, Song J, Ko HW, Choi YH, Chin YW (2017). Mangosteen extract prevents dextran sulfate sodium-induced colitis in mice by suppressing NF-κB activation and inflammation. J Med Food 20: 727–733.

Chang MZ, Zhang B, Tian Y, Hu M, Zhang GJ, Di ZL *et al*. (2016). AGEs decreased SIRT3 expression and SIRT3 activation protected AGEs-induced EPCs' dysfunction and strengthened anti-oxidant capacity. Inflammation 40: 473–485.

Chen CJ, Fu YC, Yu W, Wang W (2013). SIRT3 protects cardiomyocytes from oxidative stress-mediated cell death by activating NF-κB. Biochem Biophys Res Commun 430: 798–803.

Chen LG, Yang LL, Wang CC (2008). Anti-inflammatory activity of mangostins from *Garcinia mangostana*. Food Chem Toxicol 46: 688–693.

Choi YH, Han SY, Kim YJ, Kim YM, Chin YW (2014). Absorption, tissue distribution, tissue metabolism and safety of alpha-mangostin in mangosteen extract using mouse models. Food Chem Toxicol 66: 140–146.

Christy RJ, Yang VW, Ntambi JM, Geiman DE, Landschulz WH, Friedman AD *et al*. (1989). Differentiation-induced gene expression in 3T3-L1 preadipocytes: CCAAT/enhancer binding protein interacts with and activates the promoters of two adipocyte-specific genes. Genes Dev 3: 1323–1335.

Curtis MJ, Bond RA, Spina D, Ahluwalia A, Alexander S, Giembycz MA *et al*. (2015). Experimental design and analysis and their reporting: new guidance for publication in BJP. Br J Pharmacol 172: 3461–3471.

Delerive P, Fruchart J-C, Staels B (2001). Peroxisome proliferator-activated receptors in inflammation control. J Endocrinol 169: 453–459.

Fan XL, Zhang YH, Dong HQ, Wang BY, Ji HQ, Liu X (2015). Trilobatin attenuates the LPS-mediated inflammatory response by suppressing the NF-κB signaling pathway. Food Chem 166: 609–615.

Gutierrez-Orozco F, Failla ML (2013). Biological activities and bioavailability of mangosteen xanthones: a critical review of the current evidence. Forum Nutr 5: 3163–3183.

Harding SD, Sharman JL, Faccenda E, Southan C, Pawson AJ, Ireland S *et al*. (2018). The IUPHAR/BPS Guide to PHARMACOLOGY in 2018: updates and expansion to encompass the new guide to IMMUNOPHARMACOLOGY. Nucl Acids Res 46: D1091–D1106.

Hommes D, Peppelenbosch M, Van Deventer S (2003). Mitogen activated protein (MAP) kinase signal transduction pathways and novel anti-inflammatory targets. Gut 52: 144–151.

Hosogai N, Fukuhara A, Oshima K, Miyata Y, Tanaka S, Segawa K *et al*. (2007). Adipose tissue hypoxia in obesity and its impact on adipocytokine dysregulation. Diabetes 56: 901–911.

Johnson GL, Lapadat R (2002). Mitogen-activated protein kinase pathways mediated by ERK, JNK, and p38 protein kinases. Science 298: 1911–1912.

Joo YE, Karrasch T, Mühlbauer M, Allard B, Narula A, Herfarth HH *et al*. (2009). Tomato lycopene extract prevents lipopolysaccharide-induced NF-κB signaling but worsens dextran sulfate sodium-induced colitis in NF-κB EGFP mice. PLoS one 4: e4562.

Kanda H, Tateya S, Tamori Y, Kotani K, Hiasa K-i, Kitazawa R *et al*. (2006). MCP-1 contributes to macrophage infiltration into adipose tissue, insulin resistance, and hepatic steatosis in obesity. J Clin Invest 116: 1494–1505.

Karkeni E, Marcotorchino J, Tourniaire F, Astier J, Peiretti F, Darmon P *et al*. (2015). Vitamin D limits chemokine expression in adipocytes and macrophage migration *in vitro* and in male mice. Endocrinology 156: 1782–1793.

Kilkenny C, Browne W, Cuthill IC, Emerson M, Altman DG, Group NCRRGW (2010). Animal research: reporting *in vivo* experiments: the ARRIVE guidelines. Br J Pharmacol 160: 1577–1579.

Kim M, Lee JS, Oh JE, Nan J, Lee H, Jung HS *et al*. (2015). SIRT3 overexpression attenuates palmitate-induced pancreatic β-cell dysfunction. PloS one 10: e0124744.

Kohn AD, Summers SA, Birnbaum MJ, Roth RA (1996). Expression of a constitutively active Akt Ser/Thr kinase in 3T3-L1 adipocytes stimulates glucose uptake and glucose transporter 4 translocation. J Biol Chem 271: 31372–31378.

Koyama T, Kume S, Koya D, Araki S-I, Isshiki K, Chin-Kanasaki M *et al*. (2011). SIRT3 attenuates palmitate-induced ROS production and

inflammation in proximal tubular cells. Free Radic Bio Med 51: 1258–1267.

Lazennec G, Richmond A (2010). Chemokines and chemokine receptors: new insights into cancer-related inflammation. Trends Mol Med 16: 133–144.

Lin LG, Lee JH, Buras ED, Yu KJ, Wang RT, Smith CW *et al*. (2016). Ghrelin receptor regulates adipose tissue inflammation in aging. Aging 8: 178–191.

Lin LG, Pang WJ, Chen KY, Wang F, Gengler J, Sun YX *et al*. (2012). Adipocyte expression of PU. 1 transcription factor causes insulin resistance through upregulation of inflammatory cytokine gene expression and ROS production. Am J Physiol Endocrinol Metab 302: E1550–E1559.

Liu JX, Li D, Zhang T, Tong Q, Ye RD, Lin LG (2017). SIRT3 protects hepatocytes from oxidative injury by enhancing ROS scavenging and mitochondrial integrity. Cell Death Dis 8: e3158.

Liu QY, Li D, Wang AQ, Dong Z, Yin S, Zhang QW *et al*. (2016). Nitric oxide inhibitory xanthones from the pericarps of *Garcinia mangostana*. Phytochemistry 131: 115–123.

Lumeng CN, Bodzin JL, Saltiel AR (2007). Obesity induces a phenotypic switch in adipose tissue macrophage polarization. J Clin Investig 117: 175–184.

Mantovani A, Sica A, Sozzani S, Allavena P, Vecchi A, Locati M (2004). The chemokine system in diverse forms of macrophage activation and polarization. Trends Immunol 25: 677–686.

Marcotorchino J, Romier B, Gouranton E, Riollet C, Gleize B, Malezet-Desmoulins C *et al*. (2012). Lycopene attenuates LPS-induced TNF-α secretion in macrophages and inflammatory markers in adipocytes exposed to macrophage-conditioned media. Mol Nutr Food Res 56: 725–732.

McArdle MA, Finucane OM, Connaughton RM, McMorrow AM, Roche HM (2013). Mechanisms of obesity-induced inflammation and insulin resistance: insights into the emerging role of nutritional strategies. Front Endocrinol 4: 52.

McGrath JC, Lilley E (2015). Implementing guidelines on reporting research using animals (ARRIVE etc.): new requirements for publication in BJP. Br J Pharmacol 172: 3189–3193.

Mohamed-Ali V, Goodrick S, Rawesh A, Katz D, Miles JM, Yudkin J *et al*. (1997). Subcutaneous adipose tissue releases interleukin-6, but not tumor necrosis factor-α, *in vivo* 1. J Clin Endocrinol Metabol 82: 4196–4200.

Planavila A, Rodríguez-Calvo R, Jové M, Michalik L, Wahli W, Laguna JC *et al*. (2005). Peroxisome proliferator-activated receptor β/δ activation inhibits hypertrophy in neonatal rat cardiomyocytes. Cardiovasc Res 65: 832–841.

Qian ZJ, Wu ZQ, Huang L, Qiu HL, Wang LY, Li L *et al*. (2015). Mulberry fruit prevents LPS-induced NF-κB/pERK/MAPK signals in macrophages and suppresses acute colitis and colorectal tumorigenesis in mice. Sci Rep 5: 17348.

Shoelson SE, Lee J, Goldfine AB (2006). Inflammation and insulin resistance. J Clin Invest 116: 1793–1801.

Soromou LW, Chen N, Jiang L, Huo M, Wei M, Chu X *et al*. (2012). Astragalin attenuates lipopolysaccharide-induced inflammatory responses by down-regulating NF-κB signaling pathway. Biochem Biophys Res Commun 419: 256–261.

Suganami T, Tanimoto-Koyama K, Nishida J, Itoh M, Yuan X, Mizuarai S *et al*. (2007). Role of the Toll-like receptor 4/NF-κB pathway in saturated fatty acid–induced inflammatory changes in the interaction between adipocytes and macrophages. Arterioscler Thromb Vasc Biol 27: 84–91.

Sundaresan NR, Gupta M, Kim G, Rajamohan SB, Isbatan A, Gupta MP (2009). Sirt3 blocks the cardiac hypertrophic response by augmenting Foxo3a-dependent antioxidant defense mechanisms in mice. J Clin Invest 119: 2758–2771.

Syam S, Bustamam A, Abdullah R, Sukari MA, Hashim NM, Mohan S *et al*. (2014). β Mangostin suppress LPS-induced inflammatory response in RAW264.7 macrophages *in vitro* and carrageenan-induced peritonitis *in vivo*. J Ethnopharmacol 153: 435–445.

Tewtrakul S, Wattanapiromsakul C, Mahabusarakam W (2009). Effects of compounds from *Garcinia mangostana* on inflammatory mediators in RAW264.7 macrophage cells. J Ethnopharmacol 121: 379–382.

van der Heijden RA, Sheedfar F, Morrison MC, Hommelberg PP, Kor D, Kloosterhuis NJ *et al*. (2015). High-fat diet induced obesity primes inflammation in adipose tissue prior to liver in C57BL/6j mice. Aging 7: 256–268.

Vitseva OI, Tanriverdi K, Tchkonia TT, Kirkland JL, McDonnell ME, Apovian CM *et al*. (2008). Inducible Toll-like receptor and NF-κB regulatory pathway expression in human adipose tissue. Obesity 16: 932–937.

Wang AQ, Wang SP, Jiang Y, Chen MW, Wang YT, Lin LG (2016). Bioassay guided identification of hepatoprotective polyphenols from *Penthorum chinense* Pursh on *t*-BHP induced oxidative stress injured L02 cells. Food Funct 7: 2074–2083.

Wang Z, Lee Y, Eun JS, Bae EJ (2014). Inhibition of adipocyte inflammation and macrophage chemotaxis by butein. Eur J Pharmacol 738: 40–48.

Watanabe Y, Nagai Y, Honda H, Okamoto N, Yamamoto S, Hamashima T *et al*. (2016). Isoliquiritigenin attenuates adipose tissue inflammation *in vitro* and adipose tissue fibrosis through inhibition of innate immune responses in mice. Sci Rep 6: 23097.

Weisberg SP, McCann D, Desai M, Rosenbaum M, Leibel RL, Ferrante AW (2003). Obesity is associated with macrophage accumulation in adipose tissue. J Clin Invest 112: 1796–1808.

Wellen KE, Hotamisligil GS (2005). Inflammation, stress, and diabetes. J Clin Invest 115: 1111–1119.

Wellen KE, Hotamisligil GS (2003). Obesity-induced inflammatory changes in adipose tissue. J Clin Invest 112: 1785–1788.

Xu H, Hertzel AV, Steen KA, Bernlohr DA (2016). Loss of fatty acid binding protein 4/aP2 reduces macrophage inflammation through activation of SIRT3. Mol Endocrinol 30: 325–334.

Xu J, Zhang Y, Xiao Y, Ma S, Liu Q, Dang S *et al*. (2013). Inhibition of 12/15-lipoxygenase by baicalein induces microglia PPARβ/δ: a potential therapeutic role for CNS autoimmune disease. Cell Death Dis 4: e569.

Yuan M, Konstantopoulos N, Lee J, Hansen L, Li ZW, Karin M *et al*. (2001). Reversal of obesity-and diet-induced insulin resistance with salicylates or targeted disruption of Ikkβ. Science 293: 1673–1677.

Zeyda M, Stulnig TM (2007). Adipose tissue macrophages. Immunol Lett 112: 61–67.

Zhuge F, Ni YH, Nagashimada M, Nagata N, Xu L, Mukaida N *et al*. (2016). DPP-4 inhibition by linagliptin attenuates obesity-related inflammation and insulin resistance by regulating M1/M2 macrophage polarization. Diabetes 65: 2966–2979.

Supporting Information

Additional Supporting Information may be found online in the supporting information tab for this article.

https://doi.org/10.1111/bph.14162

Table S1 Real-Time PCR primer sequences.
Table S2 Antibodies for immunoblotting.
Table S3 Compounds isolated from the pericarps of *Garcinia mangostana*
Figure S1 Top: The chemical profile of TPX analyzed by HPLC-UV. The accurately weighed TPX was dissolved in methanol (100 μg·mL^{-1}) and sonicated for 1 h. After filtered by 0.45 μm Millipore membrane, 20 μL filtration was injected into an Agilent SB C18 column (250 × 4.6 mm, 5 μm) which was maintained at 35 °C for gradient elution with water (A) and acetonitrile (B). The elution program was set as follows: 0-40 min, 95-0% A, 5-100% B. The detection wavelength was set at 254 nm. Representative chromatogram was analyzed using a Waters Empower system and the purity of TPX (99.8%) was determined by the peak area. Bottom: ^{1}H NMR spectrum for TPX recorded in *d*6-DMSO. NMR spectrum was recorded on an ASCEND 600 MHz/54 mm NMR spectrometer. The chemical shift (δ) values are given in ppm with tetramethylsilane as internal standard, and coupling constants (*J*) are in Hz.
Figure S2 Screening of xanthones in LPS stimulated RAW264.7 cells. Cells were treated with different compounds from *G. mangostana*, ranging from 1.25 to 20 μM in the presence of LPS (1 μg·mL^{-1}). (A) NO production was determined using Griess reagent. (B) The levels of IL-6 were determined by ELISA kit. (C, D) The cytotoxicity of TPX on RAW264.7 cells with or without LPS. RAW264.7 cells were treated with TPX ranging from 5 to 20 μM in the presence or absence of LPS (1 μg·mL^{-1}) for 24 h. Cell viability was determined by MTT assay. Data are normalized to the mean value of control group. **1**, 1.25 μM; **2**, 20 μM; **3**, 20 μM; **4**, 5 μM; **5**, 5 μM; **6**, 2.5 μM; **7**, 2.5 μM; **8**, 5 μM; **9**, 10 μM; **10**, 2.5 μM; **11**, 5 μM; **12**, 1.25 μM; **13**, 1.25 μM; **14**, 2.5 μM. Data are expressed as means ± SEM ($n = 9$). #$P < 0.05$ versus DMSO, *$P < 0.05$ versus LPS.
Figure S3 TPX inhibited LPS-induced COX-2 expression in RAW264.7 cells. (A) Cells were pretreated with the vehicle or TPX (20 μM) for 1h before treatment with LPS (1 μg·mL^{-1}) for 6 h. The mRNA level of COX-2 was analyzed by real-time RT-PCR, normalized by 18S. (B) The protein level of COX-2 was detected by Western blot analysis. Data are normalized to the mean value of LPS group. GAPDH was used as an internal loading control. Data are expressed as means ± SEM ($n = 6$). #$P < 0.05$ versus DMSO, *$P < 0.05$ versus LPS.
Figure S4 Transwell assay of macrophage migration. (A) Representative images of migrated macrophages in Figure 5A. (B) Representative images of migrated macrophages in Figure 5B.
Figure S5 Effects of TPX on body weight in LPS-treated mice. Data are expressed as means ± SEM ($n = 7$).
Figure S6 The protein expressions of PPARs were determined by Western blotting and GAPDH was used as an internal loading control. Data are normalized to the mean value of LPS group. Data are expressed as means ± SEM ($n = 5$). #$P < 0.05$ versus DMSO, *$P < 0.05$ versus LPS.
Figure S7 Schematic diagram of the *in vitro* experimental designs.